Polymer Chemistry

PAPER

Check for updates

Investigation of the dynamic behavior of metallopolymers by combined experimental and theoretical methods

Milena Jäger, [a,b] Michael Freduah Agyemang, [c,d,e] Wanja T. Schulze, [c] Julian Kimmig, [a,b] Thomas Bätz, [a,b] Chiara Wondraczek, [c] Stefan Zechel, [a,b,g,h] Alexander Croy, [c] Michael Schmitt, [c,d] Jürgen Popp, [c,d,e] Stefanie Gräfe, [c,d,f] Martin D. Hager *[a,b,g,h] and Ulrich S. Schubert *[a,b,d,g,h]

In this study, we investigate the structural changes in dynamic metallopolymers during stimulus application, *i.e.* thermal treatment. For this purpose, we focused on the synthesis of polymers containing terpyridine moieties as ligands in the side chains that were complexed with either iron(II) or zinc(II) salts. The resulting crosslinked metallopolymers were characterized using differential scanning calorimetry (DSC), thermogravimetric analysis (TGA) and elemental analysis (EA). Rheology experiments, including dynamic mechanical thermal analysis (DMTA), frequency sweeps, stress relaxation and time−temperature superposition were conducted to study the stimuli-responsive mechanical properties. Hereby, the activation energy determined by stress relaxation as a combination of the metal complex and the polymer matrix could be determined. Additionally, computational master curves were obtained and the resulting relaxation spectra were analyzed. Beside the macroscopic material properties, temperature-dependent Raman spectroscopy and density functional theory (DFT) calculations were utilized to gain information on the changes on the molecular level. In this context, morphological changes in the polymer matrix were observed, which might be correlated to the presence of supramolecular aggregates. The changes on the molecular level could be linked to the macroscopic properties.

Introduction

In nature, metal complexes play an integral part in biological processes. For example, in hemoglobin or chlorophyll, the incorporation of a metal ion in the organic framework leads to unique functions like oxygen transport or photosynthesis.[1–3] Inspired by these examples, synthetic polymers have become a widely researched field. Today, polymers are applied in various areas of the society, such as in medicine,[4] in packaging[5] or as electronic devices.[6] However, traditional polymers are characterized by static and largely unalterable properties. Hence, the field of polymer research has advanced from static structures to dynamic materials.[7] These kinds of polymers belong to an interesting class of materials that are capable of undergoing reversible and controlled changes in their properties due to different internal or external stimuli.[8–10] In general, dynamic polymers can be divided into two groups, the dynamic covalent[11] and the dynamic supramolecular polymers.[12] Covalent polymers are considered dynamic when it is possible to break and to reform the bonds reversibly.[13] This can be achieved by a variety of literature known reactions, such as the thermally reversible Diels–Alder reaction,[14–16] the transesterification[17,18] or the hydrolysis of boronic esters,[19,20] the thermal structural reorganization of alkoxyamines,[21,22] the degenerative imine bond exchange,[23,24] the disulfide metathesis[25,26] or the reorganization of hindered urea bonds.[27,28] In contrast, dynamic supramolecular polymers can be based on hydrogen bonds,[29,30] host–guest interactions,[31,32] π–π stacking[33,34] or metallo-supramolecular interactions.[35,36] The usage of hydrogen bonds or π–π stacking in the design of

a Laboratory of Organic and Macromolecular Chemistry (IOMC), Friedrich Schiller University Jena, Humboldtstr. 10, 07743 Jena, Germany.
E-mail: ulrich.schubert@uni-jena.de, martin.hager@uni-jena.de
b Jena Center for Soft Matter (JCSM), Friedrich Schiller University Jena, Philosophenweg 7, 07743 Jena, Germany
c Institute of Physical Chemistry (IPC), Friedrich Schiller University Jena, Helmholzweg 4, 07743 Jena, Germany
d Abbe Center of Photonics (ACP), Friedrich Schiller University Jena, Albert-Einstein-Straße 6, 07745 Jena, Germany
e Leibniz Institute of Photonic Technology, Albert-Einstein-Straße 9, 07745 Jena, Germany
f Fraunhofer Institute for Applied Optics and Precision Engineering, Albert-Einstein-Straße 7, 07745 Jena, Germany
g Helmholtz-Institute for Polymers in Energy Applications Jena (HIPOLE Jena), Lessingstr. 12-14, 07443 Jena, Germany
h Helmholtz Zentrum Berlin für Materialien und Energie GmbH (HZB), Hahn-Meitner-Platz 1, 14109 Berlin, Germany

supramolecular polymers leads to a rapid and reversible assembly, but the resulting materials are often sensitive to temperature or solvents, which limits the material's mechanical strength.[37,38] Host–guest interactions exhibit high selectivity and self-organization but are also sensitive to temperatures.[39] In contrast to these supramolecular binding motifs, metallopolymers are tunable and can be more resistant to moisture or higher temperatures, which leads to more robust materials and broader design possibilities.[40–44]

Furthermore, metallopolymers combine classical organic polymers with metal ions or complexes to benefit from each other's properties.[45] The advantages of the polymers like lightweight,[46] tunable properties[47] and cost-effectiveness[48] are merged with the properties of metal complexes like catalytic activity,[49] bioactivity,[50] conductivity[51] and others making these polymers an unique material class.[52–54] This combination of benefits leads to many different potential applications of metallopolymers, for example as self-healing[55,56] or shape-memory materials.[42,57,58]

There are different ways to incorporate a metal ion into the polymer structure. Ciardelli *et al.*[59] postulated three different types of metal-containing polymers. First, that metal ions can be bound to a chain of the polymer by electrostatic attraction, by coordination or by linking the metal complex as a pendant or an end group to the polymer. Second, the metal complexes can be incorporated into the polymer as part of the chain by covalent linkage or by metal ligand coordination in the main chain. Lastly, the metal ions or the complex can physically interact with the polymer chain.[59,60]

In literature, ligands are typically chosen as the building blocks to incorporate the metal ions into the polymer.[43] Therefore, bidirectional, ditopic ligands with various interactions, such as ionic bonding,[61] metal-arene complexation[62] and coordinative bonding[56] are applied. The coordinative binding of the metal ion to the ligand is the most prominent way to design metallopolymers shown in literature.[42,56,63–65] Hereby a variety of different ligands containing different heteroatoms can be applied. A highly dynamic coordination environment can be achieved by the usage of imidazole[41] or histidine-inspired ligands,[66] which leads to reversible networks.[42] Other ligands like porphyrins[67] or salens[68] can integrate new functionalities into the polymer like electronic[69,70] or optical features.[67] Furthermore, different pyridine-based ligands can be utilized, therefore mono-,[71] bi-[58] or tridentate systems[64] are applied. Here, the binding constant increases from pyridine to terpyridines, showcasing the chelating effect of those ligands.[72]

In addition to the choice of ligand, it is also crucial to select the right metal salt because it influences the properties and the dynamics of the resulting metallopolymer. Each metal ion differs in geometry, ligand field stabilization and binding strength.[73] These factors determine the dynamic nature of the resulting metallopolymer networks and affect the macroscopic behavior of the materials. Therefore, different metal ions from the p-block like Al(III)[74] or Bi(III),[75] the d-block and the f-block are typically chosen. The d-block transition metals like Fe(II/III)[76]

or Ru(II/III)[77] are more commonly used than the p-block metal ions because they offer a wide range of redox states and coordination geometries,[76,77] while the f-block lanthanide ions like Eu(III)[78] or Tb(III)[79] exhibit unique optical properties that can be used for, *e.g.*, stimuli-responsive photoluminescence.[80]

Overall, by selecting specific ligand/metal combinations, the properties can be adjusted from highly reversible, *i.e.* low binding constant of the supramolecular unit, to nearly irreversible based on a high association constant.[42,72] Applying this principle enables a tailor-made design of the materials thereof with tunable and on-demand properties.[63]

Terpyridine ligands have gained significant attention due to their coordination to transition metals featuring a high degree of versatility and an adjustable binding constant by choosing the respective metal ion.[64,65,76,81] The resulting metallopolymers can be addressed by different stimuli, *e.g.*, temperature,[57] and can be utilized for different applications as smart materials. In this context, self-healing[56,63,64] and shape-memory polymers[42,57,58] could be obtained by the utilization of this ligand.

However, the focus of previous works was on synthesizing and characterizing those materials, while there are still unanswered questions about the structural dynamics, in particular during stimulus application. Rheology experiments were also conducted before but mostly to confirm the results from self-healing[63] or shape-memory investigations.[57] In a previous study from our group, Bode *et al.*[63] confirmed the correlation between the self-healing ability and the supramolecular bond lifetime linked to the crossover points in frequency sweep measurements, while Meurer *et al.*[57] confirmed the shape-memory ability of the used metallopolymers *via* frequency sweeps and thermomechanical analysis. However, a detailed investigation of the macroscopic and molecular processes of those metallopolymers during thermal treatment is still missing preventing further optimization of such systems.

In this study, we aim to provide more in-depth detail of the structural and molecular dynamics of terpyridine-based metallopolymers using Fe(II) and Zn(II) metal ions. For this purpose, a combination of rheological investigations and Raman spectroscopy are applied. While rheology provides insights into the viscoelastic behavior and structural changes,[82] Raman spectroscopy offers a perspective on the bond interactions and coordination changes.[83] To complement these results theoretical calculations enable predictions of the molecular behavior and the structural changes.[84] With this approach, we aim to build a more complete picture of the material's response and behavior that could lead to the development of new smart materials with better and on-demand functionalities.

Results and discussion

Synthesis of the metallopolymers

In order to investigate the reversible moieties in metallopolymers, first, linear polymers featuring ligands in the side-chain were prepared. As the ligand, 6-(2,2′:6′,2″-terpyridin-4′-yloxy)-

hexyl-methacrylate (**Tpy-MA**) was selected due to its well-established coordination properties, making it particularly suitable for the metallopolymer synthesis.[42,57,58,85] The ligand was synthesized following a previously reported procedure.[86] The linear polymers were synthesized *via* reversible addition–fragmentation chain-transfer (RAFT) polymerization. Methyl methacrylate (MMA, **P1**), butyl methacrylate (BMA, **P2**), or 2-ethylhexyl methacrylate (2-EHMA, **P3**) were chosen as comonomers and were polymerized together with **Tpy-MA**. Hereby, a terpyridine-content of *ca.* 10% was aimed to introduce a significant amount of coordination functionalities, to have a controlled, but not too dense crosslinking and to compare the resulting systems to literature known metallopolymers.[86] The resulting polymers were characterized using elemental analysis (EA), differential scanning calorimetry (DSC), thermogravimetric analysis (TGA), and size exclusion chromatography (SEC) (all results are depicted in the SI; see Table 1 for a summary of these). ^{1}H NMR spectroscopy confirmed a consistent incorporation of approximately 9% **Tpy-MA** across all polymers. The SEC results revealed narrow dispersity (<1.25) and similar molar masses ranging from 12 500 g mol^{-1} for **P1** to 23 500 g mol^{-1} for **P3**, as expected for the RAFT polymerization process. The glass transition temperatures (T_g) obtained from DSC measurements are similar to former results from our group.[56,85] Since similar **Tpy-MA** content, comparable molar masses and comparable degrees of polymerization were obtained, the polymers could be utilized to prepare metallopolymer networks, which are highly comparable. Afterwards, the metallopolymers were synthesized by converting the linear polymers with either $FeSO_4 \times 7 H_2O$ (**P1-Fe, P2-Fe, P3-Fe**) or Zn (TFMS)$_2$ (**P1-Zn, P2-Zn, P3-Zn**). These metal salts were dissolved in methanol and added to chloroform solutions of the polymers (see Scheme 1), exploiting the high binding affinity of the terpyridine ligands for metal ions.[87,88] All metallopolymers were characterized by EA. The determined compositions are in the expected range (see SI Table S6). DSC, and TGA (see Table 1 and SI Table S6) provided insights into the thermal properties of the metallopolymers. Unfortunately, it was not possible to determine T_g from the DSC measurements for all metallopolymers (see SI Fig. S10–S12). Hence, dynamic

mechanical thermal analysis was utilized for the determination, which will be described in a following section. For the degradation temperatures, all metallopolymers featured a lower decomposition temperature (T_d) compared to the linear polymers. For example, **P2** shows degradation at 238 °C while **P2-Fe** and **P2-Zn** exhibit a T_d of 210 °C and 215 °C, respectively. Since all metallopolymers have a first degradation between 150 °C and 270 °C they are stable enough for the switching and the following analysis. To provide additional context and to improve the understanding of the metallopolymer properties, polymer networks without ligands or metal salts were synthesized for comparison. MMA (**P1-cc**), BMA (**P2-cc**) and 2-EHMA (**P3-cc**) were crosslinked with 1,6-hexanediol dimethacrylate (HDMA) as the covalent crosslinker and the networks were obtained *via* free radical polymerization (FRP) leading to a 5% content of HDMA within the polymer, which results in a similar crosslinking density compared to the metallopolymers. These polymer networks were subsequently characterized using EA, DSC, and TGA (see Table S8) to analyze their composition, thermal behavior and stability. The determined compositions *via* EA were in the expected range. The DSC measurements revealed comparable glass transition temperatures to the linear polymers, but slightly lower values compared to the metallopolymers, while the degradation temperatures lie in the same range, which makes these networks highly useful for comparison. Furthermore, model complexes $[(Tpy)_2Fe]^{2+}$, $[(Tpy)_2Zn]^{2+}$ and poly(methyl methacrylate) (**PMMA**) were synthesized as well (see SI Tables S1 and S4).

Complexation behavior in solution

Metallopolymers and metal complexes can undergo dynamic and reversible transitions, in particular in solution.[89] Understanding the reversibility in solution is also crucial for understanding the reversible behavior in the solid state. Therefore, we firstly investigated the metal complexes, which were utilized for the metallopolymer synthesis, in solution. For this purpose, isothermal titration calorimetry (ITC) was applied, since it provides valuable insights into the binding constants of the metal complexes as it has been demonstrated in other studies.[42,57] The results of these already published

Table 1 Summary of the calculated composition, the determined molar masses and dispersities and thermal properties of the polymers **P1-P3** and the thermal properties of the metallopolymers **P1-Fe** to **P3-Zn**

| Polymer | Tpy content [%][a] | SEC[b] | | | T_d^c [°C] | T_g^d [°C] | MP | T_d^c/°C | T_g^e/°C |
		M_n/g mol^{-1}	M_w/g mol^{-1}	Đ					
P1	9.3	12 500	15 100	1.21	167	76	**P1-Fe**	148	108
							P1-Zn	162	121
P2	9.1	13 300	15 300	1.15	238	25	**P2-Fe**	210	50
							P2-Zn	215	89
P3	9.4	23 500	26 300	1.12	298	3	**P3-Fe**	223	50
							P3-Zn	268	71

[a] Determined *via* NMR spectroscopy (in CD_2Cl_2 at 300 MHz). [b] Eluent: $CHCl_3$/NEt$_3$/i-PrOH (94/4/2), PMMA standards. [c] Degradation temperatures determined *via* TGA measurements: 25 to 600 °C, 20 K min^{-1}, nitrogen atmosphere. [d] Glass transition temperatures determined *via* DSC measurements: −110 to 150 °C, 3rd heating run, 10 K min^{-1}, nitrogen atmosphere. [e] Glass transition temperatures determined *via* DMTA: 25 to 100, 130 or 150 °C, 2 K min^{-1}, 1 Hz.
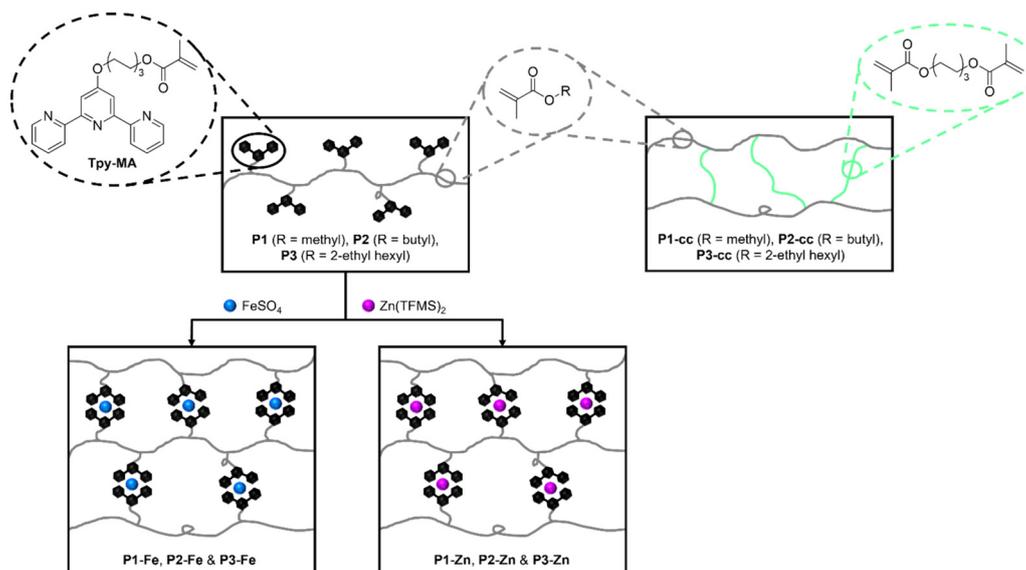
Scheme 1 Schematic representation of the synthesis of all metallopolymers **P1-Fe** to **P3-Zn** and of the polymer networks **P1-cc** to **P3-cc**.

ITC measurements for $Zn(TFMS)_2$ and $FeSO_4$ with the terpyridine ligand are summarized in Table 2.[42,57] Within these measurements, a single binding event with a stoichiometry of 2 was found for the terpyridine ligand and the used metal salts, indicating that two terpyridine units binds simultaneously to one metal ion.[42,57] Furthermore, it should be noted that the counter anions can play a significant role in the binding affinities of the complexes, which was previously discussed in literature.[63] The choice of counter anion was based on the non-binding nature of the anions to the metal ions, in contrast to, *e.g.*, chloride which acts as a bridging ligand in $Mn(II)$.[63] In addition, $FeSO_4$ and $Zn(TFMS)_2$ are both air-stable. Furthermore, the iron complex exhibits a logarithmic association constant of 23 (corresponding to the maximum measurable value with our instrument),[57] significantly higher than the 15 observed for the zinc complex.[42] Consequently, the bis-terpyridine iron(II) complex is much more stable compared to its zinc analogue. To validate these results, density functional theory (DFT) calculations were performed. The complexation of the two metal ions has been modeled with an isodesmic reaction, using zinc(II) and iron(II) ions that are explicitly coordinated by methanol molecules, which was part of the solvent mixture utilized in the ITC measurements.[57] The resulting free Gibbs energy (G_{calc}) and the association constant $\ln K_{calc}$ are summarized in Table 2.

Here, the logarithmic association constant is again higher for the bis-terpyridine iron complex with 130 compared to the zinc complex with 72, which aligns well with the ITC results. Furthermore, the free Gibbs energy was determined *via* the DFT calculations. These complex formation energies are higher for the $[(Tpy)_2Fe]^{2+}$ complex with -58 kJ mol^{-1} from experimental results and -328 kJ mol^{-1} from theoretical calculations compared to the $[(Tpy)_2Zn]^{2+}$ complex. One should mention that absolute association constants are notoriously difficult to predict, with deviations of the logarithmic constant by a factor of 2 to 10 being very common.[90–92] One cause of the reported deviations could be that the calculated values assume pure methanol as the solvent, deviating from the experiment. Additionally, it can be shown that the anion's electrostatic effect plays an important role. Table S13 displays the values for a repeated calculation with additional chloride ions to mimic the effect of the anions, showing a drastic reduction of the calculated association constants and improved alignment with the experiments. If the values for both salts are put into proportion, the result for the relative free Gibbs energies are similar for the experimental and theoretical approach. These results make the two chosen salts very suitable candidates for the formation and investigation of structural changes in metallopolymers, since one more stable and one less stable complex are analyzed.

Table 2 Summary of the calculated and experimentally determined free Gibbs energy (G), association constants (K) and stoichiometry (n) of the bis-terpyridine metal complexes

| Complex	DFT			ITC			
	G_{calc}/kJ mol^{-1}	$G_{calc}(Fe)/G_{calc}(Zn)$	$\ln K_{calc}$	G_{exp}/kJ mol^{-1}	$G_{exp}(Fe)/G_{exp}(Zn)$	$\ln K_{exp}$ [42,57]	n
$[(Tpy)_2Fe]^{2+}$	−328.277	1.81	130.306	−58.009	1.54	23.026	1.91
$[(Tpy)_2Zn]^{2+}$	−181.657		72.107	−37.767		14.991	1.90

Rheological investigation

Dynamic mechanical thermal analysis (DMTA). To structurally characterize the metallopolymers and polymer networks, firstly, dynamic mechanical thermal analyses (DMTA) were performed. For this purpose, the samples were heated up under a constant oscillating shear strain and a constant frequency (1 Hz) to study the material's response. Hereby, the maximum of the loss modulus (G'') was utilized to determine T_g of all metallopolymers (see Table 1).[93] The T_g values are higher compared to those of the linear polymers, for example **P1** has a glass transition temperature of 76 °C while the corresponding metallopolymers exhibit a T_g of 108 °C (**P1-Fe**) and 121 °C (**P1-Zn**). Furthermore, it could be observed that the storage modulus (G') remained higher compared to the loss modulus (G'') for all metallo-polymers across the entire temperature range indicating a crosslinked polymer network structure even during heating.[94] The temperature range of the measurements was chosen according to the predominant comonomer in the metallopolymers. For example, MMA has a higher T_g than 2-EHMA, therefore it was possible to go to higher temperatures without softening the sample too significantly. Consequently, the measurement was performed for MMA (**P1-Fe** and **P1-Zn**) between 25 °C and 150 °C, for BMA (**P2-Fe** and **P2-Zn**) between 25 °C and 130 °C and for 2-EHMA (**P3-Fe** and **P3-Zn**) between 25 °C and 100 °C. A representative DMTA curve for **P2-Zn** is shown in Fig. 1A, the remaining measurements are depicted in the SI (Fig. S15–S22). It should be noted that this was also the case for the polymer networks featuring a non-reversible covalent crosslinker. Furthermore, no clear difference was observable between the different comonomers, but between the Fe(II) and Zn(II) containing metallopolymers. Here, the loss factor tan(δ) shows two distinctive peaks for the iron-containing ones, **P1-Fe**, **P2-Fe** and **P3-Fe**, while for the other three metallopolymers only one peak is visible. If the two peaks are compared to the covalently crosslinked networks the first peak

aligns with the maximum of the tan(δ) of those, leading to the assumption that the first peak corresponds to the glass transition of the polymer backbone, while the second peak corresponds to the activation of the metal–ligand complex itself or aggregates of multiple complexes. This phenomenon is best visible for **P2-Fe** in Fig. S17; the first peak is around 50 °C to 60 °C where the glass transition of the BMA backbone occurs while the second signal is around 90 °C to 100 °C where it is possible to address the dynamic network. For the Zn(II) containing metallopolymers the peak only occurs at higher temperatures than the glass transition of the covalently crosslinked networks, which might be associated with a simultaneous occurrence of the glass transition and the activation of the supramolecular bond. A similar behavior of multiple signals in the tan(δ) plot can be found in literature.[95] Hence, further rheological measurements were required to observe the material's properties, which will be discussed in the following paragraphs.

Frequency sweeps. Frequency sweeps were performed for all metallopolymers and the non-reversible polymer networks at various temperatures to evaluate the stability of the bis-terpyridine complexes and to assess the thermal behavior of the supramolecular binding units. The temperatures were chosen depending on the T_g of the material. The frequency sweep curves for **P2-Zn** are exemplary shown in Fig. 1B. The other measurements are displayed in the SI, Fig. S22–S29. As seen for **P2-Zn**, a crossover of G' and G'' is visible at 120 °C and 130 °C. At higher temperatures, the crossover occurs at higher frequencies, indicating that the activation of the supramolecular network is temperature-dependent.[96] Specifically, it appears at 0.0996 rad per s at 120 °C and 0.0396 rad per s at 130 °C. This result indicates that the reversible bonds are activated. A similar behavior could also be observed for all other metallopolymers containing the bis-terpyridine zinc complex or other supramolecular polymers,[63] such as ionomers[96] or hydrogen-bond based systems.[97] However, for the metallopoly-
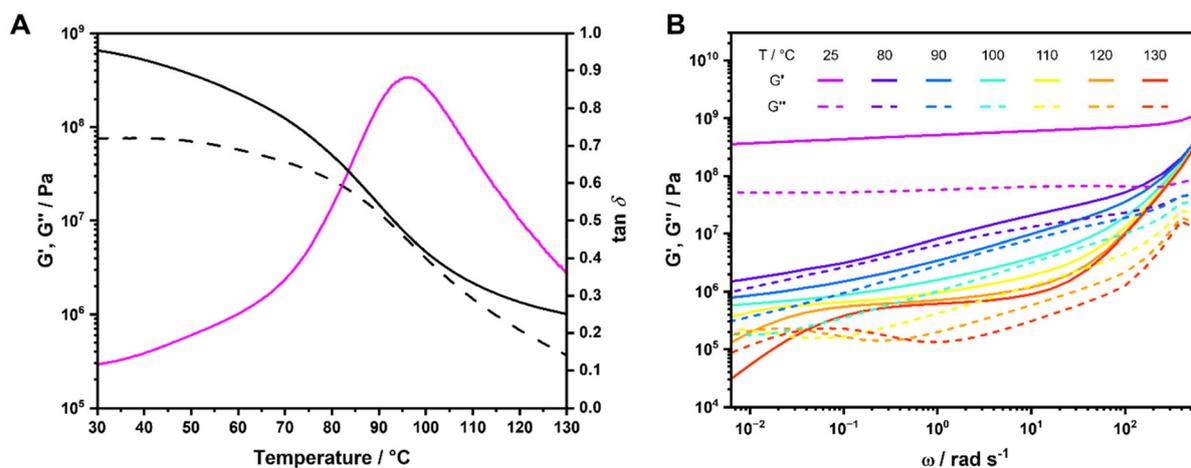
Fig. 1 Rheological plots for **P2-Zn**: (A) DMTA measurement from 25 to 130 °C with the storage modulus G' (black), the loss modulus G'' (black dotted) and the loss factor tan δ (violet), (B) frequency sweep from 0.00628 to 628 rad per s at different temperatures with storage modulus G' (solid lines) and loss modulus G'' (dotted lines).

mers containing iron, G' and G'' converge but no actual crossover occurs. This suggests that the iron complex is thermally more stable, which aligns well with the results of the ITC measurements and the higher binding constant of those complexes. Furthermore, for the covalently crosslinked polymers **P1-cc** to **P3-cc** no significant crossover occurs, which is connected to no activation of the bonds and, therefore, no significant change in the polymer structure. If the curves for the MMA, BMA and EHMA containing metallopolymers are compared, only a difference regarding the type of used metal ion is visible, while the comonomer does not have an influence on the behavior of the samples during frequency sweep measurements. Furthermore, it is possible to calculate the time of the observed crossovers of G' and G'' which can be attributed to the supra-molecular bond lifetime (τ_b)[96] or other phenomena like terminal relaxation of the polymer backbone.[98] The resulting values are summarized in Table 3. These values are similar across all metallopolymers containing zinc, revealing that the crossover in the frequency-dependent measurements originates from the complex. They decrease at higher temperatures due to the activation of the complex. This behavior has also been observed in previous studies on comparable polymers.[57] Bode *et al.*[63] presented self-healing metallopolymers containing the terpyridine ligand, BMA and different metal salts. Here, the network with $ZnCl_2$ showed a τ_b at 150 °C of 0.15 s, this value is smaller than for **P2-Zn** which features a τ_b at 130 °C of 153.6 s; however, the utilized temperature in the previous study is higher maybe leading to a lower value of τ_b. Furthermore Meurer *et al.*[57] calculated the supramolecular bond lifetime for terpolymers containing two different ligands, including the here presented terpyridine moiety. For example, the BMA containing polymer with Fe(II) and Zn(II) exhibits a τ_b at 130 °C of 89 s, which is faster than for **P2-Zn** but still in a similar range.

Stress relaxation. Another rheological method to characterize the dynamic nature of the metallopolymers are stress relaxation measurements.[99–104] These experiments refer to the gradual decrease in stress experienced by a material under constant strain over time.[105,106] Understanding stress relaxation is crucial for predicting the long-term performance and durability of polymer-based materials.[107] In our case a shear strain of 2% was applied and the temperature was varied for each measurement. The resulting plot for **P2-Zn** is displayed in Fig. 2A, and the normalized plot in Fig. 2B. The results of the other samples are depicted in the SI, Fig. S30–S52. For **P2-Zn**, the material relaxes faster over time at higher temperatures, meaning that the stress relaxation behavior is temperature dependent. This observation is valid until 80 °C and is comparable to results for other vitrimeric materials.[108] For 90 °C and 100 °C, the material relaxes slower again. This behavior can be compared to partial vitrimers, where reversible and crosslinked moieties can be found in the material, indicating that not all reversible metal complexes are activated at this temperature.[109] For the metallopolymers **P2-Fe** and **P3-Zn** a similar behavior can be observed, while the stress decreases with higher temperatures across the whole temperature range for **P1-Fe** and **P1-Zn**. This stress relaxation behavior can be typically found for vitrimers.[108] A different stress relaxation behavior can be seen for the measurements of **P3-Fe**. Here, stress relaxation turns slower for higher temperatures. For all samples, which featured a faster relaxation with higher temperatures, *i.e.* revealed a vitrimer-like behavior, the results were fitted using two different models. First, the Maxwell model (see eqn (1)) was implemented, which describes a single relaxation mode in an ideal system.[106] Here G_0 describes the initial relaxation modulus and τ the characteristic relaxation time when $1/e$ of the initial value is reached. Since materials are normally not ideal, a second model could be applied, which takes a multimodal distribution of relaxation modes into account.[106] This model is the Kohlrausch–Williams–Watts (KWW) model and describes a stretched exponential function (see eqn (2)).[110,111] Here, τ^* is the characteristic relaxation time at $1/e$ of G_0 and β is the stretching exponential. An example of both models fitted to the stress relaxation data of **P2-Zn** at 40 °C and 80 °C is depicted in Fig. 2C. Similar plots for the other metallopolymers as well as the polymer networks can be found in the SI.

$$G(t) = G_0 \exp\left(-\frac{t}{\tau}\right) \quad (1)$$

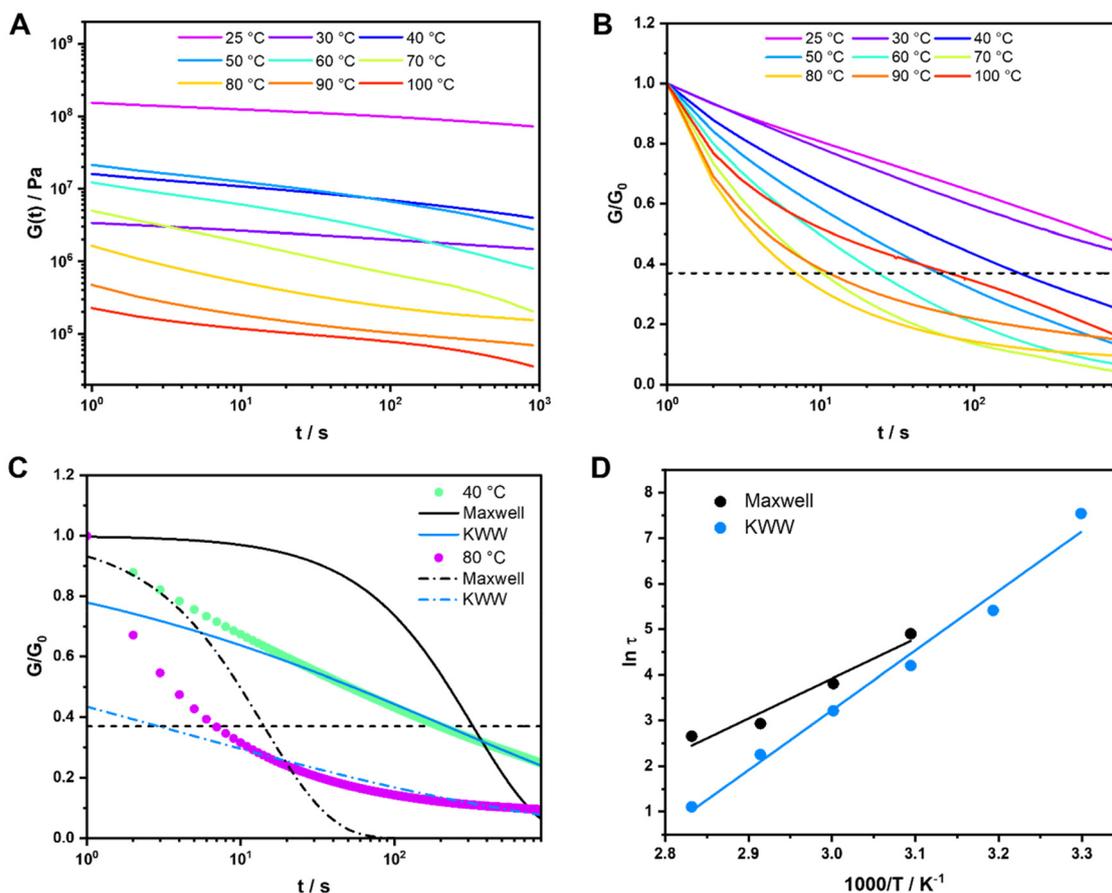$$G(t) = G_0 \exp\left(-\left(\frac{t}{\tau^*}\right)^{\beta}\right) \quad (2)$$

Fig. 2C demonstrates that the Maxwell model does not fit the measured data very well; on the other hand, the stretched exponential function from the KWW model fits the data much better, indicating that the measured samples are not ideal and simple. This is also the case for all other metallopolymers and crosslinked polymers (see SI). Since both models do not fit the measurements perfectly, it would in principle be possible to fit the stress relaxation data using a modified KWW function using a fast and a slow relaxation as shown in literature.[112]

Table 3 Summary of the determined values of the crossover times (τ_b) and the activation energies (E_A) for the synthesized metallopolymers and polymer networks

Sample	$T/°C$	τ_b/s	E_A (Maxwell)/kJ mol^{-1}	E_A (KWW)/kJ mol^{-1}
P1-Fe		n.d.^{a}	94.8	132
P1-Zn	130	442.5	106	120
	140	465.1		
		242.1		
		20.6		
		0.28		
P2-Fe		n.d.^{a}	90.3	94.3
P2-Zn	120	561.8	75.5	109
	130	153.6		
P3-Zn	110	666.7	41.0	42.0
	120	190.1		
P1-cc		n.d.^{a}	100	131
P2-cc		n.d.^{a}	81.5	124

^{a} Not detectable.

Fig. 2 Stress relaxation plots for **P2-Zn**: (A) stress relaxation measurement from 25 to 100 °C, (B) normalized stress relaxation plot, (C) normalized plot of the stress relaxation measurements at 40 and 80 °C fitted using the Maxwell and KWW models and (D) Arrhenius plot for Maxwell and KWW models.

However, in the following section we report that the presented metallopolymers exhibit multiple, *i.e.* five to seven, relaxation modes. Therefore, it is not possible to only use a single or a two-term fitting for these plots. Hence, the Maxwell model (eqn (1)) and the KWW model (eqn (2)) are depicted, even though we exhibit more than one relaxation. To compare both shown approaches the following calculations were performed for both models. Using τ from the Maxwell model and τ^* from the KWW model, it is possible to calculate the activation energies (E_A). Therefore, the Arrhenius correlation of E_A was utilized (see eqn (3)).[113]

$$\ln \tau(t) = \ln \tau_0 + \frac{E_A}{RT} \quad (3)$$

The resulting Arrhenius plots of **P2-Zn** in a temperature range from 50 °C to 80 °C for the Maxwell model and from 30 °C to 80 °C for the KWW model are presented in Fig. 2D and for the additional metallopolymers and polymer networks in the SI, Fig. S53–S58. Furthermore, the calculated activation energies are summarized in Table 3. The found E_A values range from 132.0 kJ mol^{-1} (**P1-Fe**) to 41.0 kJ mol^{-1} (**P3-Zn**) for the metallopolymers. These values are in the range of acti-

vation energies found for other vitrimers[114] and are comparable to the free Gibbs energies determined *via* ITC measurements (see Table 2). However, the values are significantly smaller compared to those of the DFT-modeled Gibbs free energies (Table 2). For **P3-Fe** it was not possible to determine E_A because the relaxation did not follow a vitrimeric behavior. As shown in Table 3 the E_A values differ a lot comparing the results from Maxwell and KWW fits. In general, all values for KWW are higher compared to Maxwell. The values for the metallopolymers containing MMA (**P1-Fe** and **P1-Zn**) are higher than the ones containing BMA (**P2-Fe** and **P2-Zn**) or 2-EHMA (**P3-Zn**). Only for the MMA-containing metallopolymers, the one containing iron exhibits a higher activation energy compared to its counterpart metallopolymers containing zinc. This result has already been described by the theoretical calculations of the free Gibbs energy (see Table 2) and is also in line with the complexation behavior in solution. However, this is not the case for the other metallopolymers. Another observation is that the E_A values determined by the Maxwell and KWW approach of **P1-cc** and **P2-cc** lie in the same range as their corresponding metallopolymers **P1-Fe**, **P1-Zn** and **P2-Fe**, **P2-Zn**, respectively. The comparison to the co-

valently crosslinked networks reveal that the polymer matrix has a significant influence on the activation energy determined by the stress relaxation measurements. These results lead to the assumption that the resulting E_A values are a combination of the activation of the metal–ligand complex and the T_g of the polymer matrix. Another approach to analyze the stress relaxation measurements is to construct a master curve using the time–temperature superposition principle.[115] Hereby, the resulting curve was fitted using the KWW equation (eqn (2)) and the resulting shift factors a_T could be correlated to the τ^* values to calculate the activation energy. The resulting plots are depicted in the SI (Fig. S59–S69) and the E_A values are summarized in Table S9. However, not all master curves follow the KWW equation very well, which leads to unrealistic E_A values, e.g., for **P3-Zn**, where an activation energy of 228 kJ mol^{-1} was obtained while only a value of 42 kJ mol^{-1} could be determined using the previously described KWW approach. Furthermore, these findings suggest that stress relaxation measurements are not the best method to clarify the structural properties of metallopolymers, i.e. the supramolecular binding motifs of the used bis-terpyridine metal complexes.

Time–temperature superposition. Since the conducted frequency sweep measurements revealed the most promising results for the understanding of the structural changes in the metallopolymers, time–temperature superposition (TTS) was performed. The TTS principle is based on the fact that the measured data, here G' and G'', are temperature dependent.[116] This relationship indicates that a change in temperature leads to both horizontal and vertical shifts of the frequency sweep results. The materials, for which such a time–temperature-shift is applicable, are called thermorheologically simple.[117] This procedure solves the problem of a limited frequency range and it is possible with the use of the resulting master curves to predict the material's behavior over a larger time scale.[118,119] A similar approach was also performed for other reversible polymers in literature.[110,119–126] To check if the TTS principle is applicable for the metallopolymers and the irrever-

sibly crosslinked polymer networks, modified Cole–Cole plots were obtained at first. These plots are almost temperature independent and should overlap.[121,127] The Cole–Cole plot of **P2-Zn** is exemplary shown in Fig. 3A. Here, the values of G' and G'' at different temperatures in an angular frequency range from 0.00628 rad per s to 6.28 rad per s were utilized. This plot confirms a complete overlap of the two variables, so TTS should be applicable. Similar results were also obtained for the other metallopolymers and the irreversibly crosslinked polymer networks. These plots are depicted in the SI (Fig. S70–S77). The slopes within these plots could be determined. For **P2-Zn** (see Fig. 3A) the slope increases with increasing temperature from 0.75 to 1.98, reaching almost the value of 2, which Han et al. postulated as the value for an ideal non-crosslinked polymer.[127] Therefore, at 120 °C and 130 °C the supramolecular crosslinking points are highly activated, which correlates to the observed crossover points in the frequency sweep measurements. Since the value of 2 is not reached completely, some crosslinking points are not activated. Alternatively, the reversibility could also be based on an associated mechanism, which results in a polymer network with exchangeable bonds. This hypothesis is supported by the DMTA measurements (see above), in which G' is always higher than G''. However, for all other metallopolymers (see SI), such high values could not be obtained. Nevertheless, the values are always higher compared to the ones of the irreversibly crosslinked polymer networks, indicating that the reversibility in the supramolecular polymers is higher, which is associated with the dynamic metal–ligand interaction. Subsequently, master curves were constructed. A reference temperature (T_{ref}) was chosen for every sample, for **P2-Zn** 110 °C was chosen as the reference temperature since it is in the middle of the temperature range (this approach was always performed for the other samples).[117] The curves were shifted horizontally using shift factors a_T and no vertical shifting (b_T) was required in this case. This means that **P2-Zn** is a non-complex polymer in the mean of the TTS.[117] The resulting master curve is shown in Fig. 3B. The other
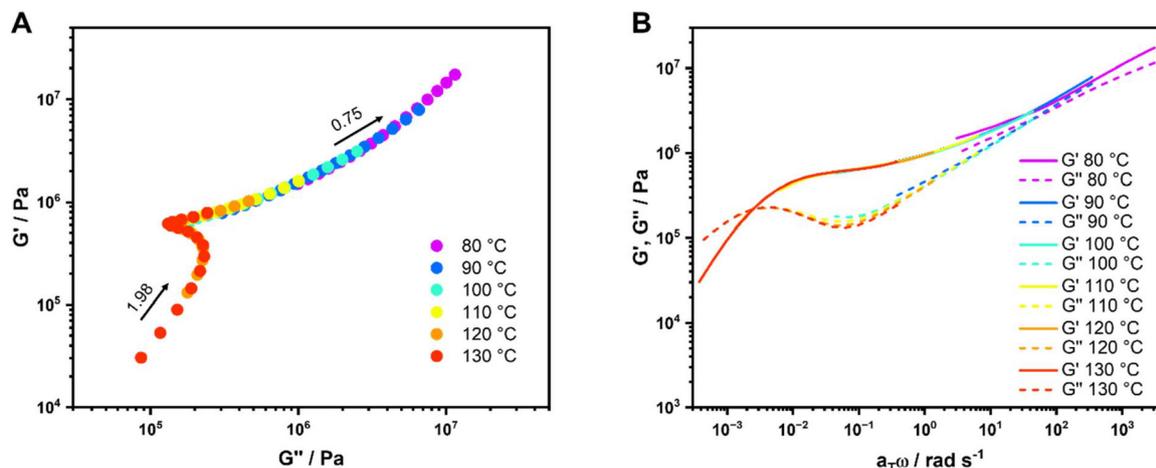

Fig. 3 (A) Modified Cole−Cole plot of **P2-Zn**, (B) TTS master curve of **P2-Zn** at T_{ref} = 110 °C.

Table 4 Summary of the reference temperatures (bold and underlined) and shift factors a_T and b_T for the master curves and the material constants C_1 and C_2 from the WLF-equation for all metallopolymers and polymer networks

Sample								WLF C_1	WLF C_2/°C
P1-Fe	T/°C	100	110	__120__	130	140		28.71	174.91
	a_T	3000	59	1	0.027	0.0015			
	b_T	0.85	1	1	1	1			
P1-Zn	T/°C	100	110	__120__	130	140		9.84	68.38
	a_T	3000	55	1	0.05	0.01			
	b_t	0.9	1	1	1	1			
P2-Fe	T/°C	40	50	60	__70__	80	90	13.99	180.26
	a_T	800	56	6.5	1	0.18	0.043		
P2-Zn	T/°C	80	90	100	__110__	120	130	8.15	109.85
	a_T	490	55	7	1	0.21	0.06		
P3-Fe	T/°C	40	50	60	__70__	80	90	10.20	141.44
	a_T	380	45	6.1	1	0.21	0.06		
P3-Zn	T/°C	70	80	90	__100__	110	120	31.75	619.72
	a_T	150	15	3	1	0.3	0.1		
P1-cc	T/°C	90	100	110	__120__	130	140	4.56	63.90
	a_T	4500	120	7	1	0.23	0.1		
	b_T	0.85	0.9	0.95	1	1.05	1.1		

master curves are presented in the SI, Fig. S78–S85, and a summary of the used shift factors and reference temperatures is provided in Table 4. Here, it should be noted that only a vertical shift using the shift factors b_T was required for the samples containing MMA, suggesting that these samples exhibit more thermorheologically complex behavior.[128] All master curves fit very well, which means that it is possible to predict the material's behavior over a longer time frame.[117] To validate the master curves, van Gurp-Palmen plots were constructed,[129] which are presented in the SI (Fig. S86–S94). All samples, except the ones containing MMA as a comonomer, show a good overlap. The reduced overlap for **P1-Fe**, **P1-Zn** and **P1-cc** reflect the necessity to apply the vertical shift factor b_T in the construction of the master curve. Generally, there are different models available for the TTS evaluation.[130–132] The most common one is the Williams-Landel-Ferry (WLF) model.[117] The WLF-equation (eqn (4))[133] is an empirical model based on Doolittle's mean free volume equation and Arrhenius kinetics. It is applicable within the temperature range of T_g to $(T_g + 100 \text{ K})$.[133]

$$\log a_t = \log\left(\frac{\eta}{\eta_r}\right) = -\frac{C_1(T - T_r)}{C_2 + (T - T_r)} \qquad (4)$$

In this equation two material constants C_1 and C_2, often described as the WLF parameters, are utilized, while T_r is the reference temperature for generating the master curve.

For this study, the measurements were conducted around T_g so the WLF-equation is applicable. The WLF parameters C_1 and C_2 were determined *via* linear plotting (see SI, Fig. S95–S103). The results of this analysis are presented in Table 4. The WLF parameters vary significantly and there is no clear trend in comparison between the metal ions used. Overall, the TTS principle is a good way to analyze the metallopolymers, but no other structural changes than in the frequency sweeps (*i.e.* activation of the complexes at higher temperatures) could be determined.

Computational rheology. To further characterize the dynamic behavior of the metallo-polymers, computational rheology[134] was applied, which refers to the calculation of the master curve and the relaxation spectrum using the experimentally determined frequency sweep data. For this purpose, we established the RheoSpec program (see SI).[135–137] First, the results from the frequency measurements were utilized to calculate the corresponding master curve, an example is shown for **P2-Zn** in Fig. 4A. The computational master curve looks almost identical compared to the constructed one shown in the previous section. This is also the case for all other samples. The corresponding computational master curves are shown in Fig. S104–S111. It should be noted that for the computational master curves the shift factor b_T was neglected and only the shift factor a_T was used.

For better understanding of the master curves, we decided to model relaxation spectra $H(\tau)$[134,138] using the RheoSpec program. These plots reveal the underlying relaxation modes that cannot be seen in any other measurements. Since the derivation of $H(\tau)$ from the frequency sweep measurements of the storage and loss modulus over a limited frequency range is hard, it is only possible to calculate an approximate function, because small changes in G' and G'' from the experimental data lead to variations in the relaxation spectrum.[137]

There are two different methods for the use of relaxation spectra, the discrete[139] and the continuous mode.[140] We used the continuous mode, since it is a more compact method to study the underlying relaxation responses.[135,137] The resulting spectra of the samples can be found in SI (Fig. S113–S121). For a better understanding of this data, a comparison between the samples with the same comonomer and the samples containing the same metal salt were carried out (see Fig. 4B and Fig. S122–S125). In Fig. 4B all samples containing MMA as the comonomer are summarized, here all three relaxation curves look very similar. **P1-Fe** and **P1-Zn** look almost identical, the sample containing Zn(ɪɪ) is just shifted slightly to longer times.
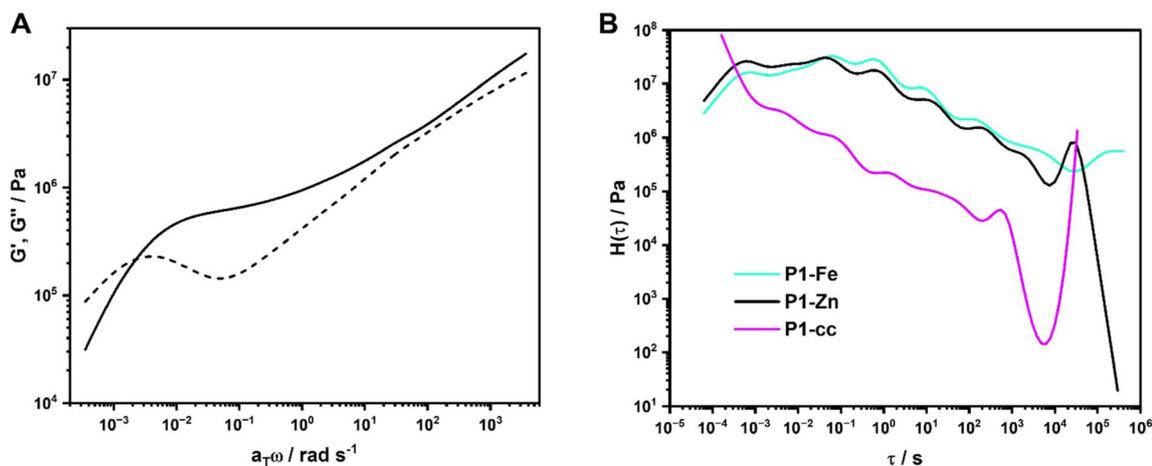
Fig. 4 (A) Computational master curve of **P2-Zn** at T_{ref} = 120 °C, (B) computational relaxation spectrum of **P1-Fe**, **P1-Zn** and **P1-cc**.

Since the frequency sweep measurements were performed up to 140 °C, the T_g of PMMA is quite close, this leads to a better resolution in the relaxation spectra. For the samples containing BMA and 2-EHMA as a comonomer (see SI, Fig. S122 and S123) the T_g is lower, and the conducted temperature range in the frequency sweep measurements are much higher compared to the glass transition temperature. As for those samples, there is no clear difference between the relaxation curves. Furthermore, when comparing all samples containing Fe(II) (see Fig. S124) or Zn(II) (see Fig. 4B) no clear distinction between the BMA- and 2-EHMA-containing metallopolymers is possible.

There are about seven different peaks in the $H(\tau)$ spectrum for the MMA-containing samples and around five to six peaks for the BMA- and EHMA-containing samples. This leads to the conclusion that the metallopolymers are very complex materials and there are multiple relaxations visible for the metal–ligand complex itself and the polymer backbone. In literature, there are often only two distinctive peaks shown in the $H(\tau)$ spectra that could be assigned to distinctive relaxation processes.[141–143] However, there are also examples of polymers featuring more complex behavior, like polyimides[134] or polyurethanes.[144]

Raman spectroscopy and DFT modelling

Raman spectroscopy is a labelfree analytical technique that provides highly specific molecular information. It has extensively been applied to study ligand binding, complexation, and structural changes in various systems.[57,85,145] Building on its well-established molecular specificity, Raman spectroscopy is used in this study to validate the formation of metal complexes within the polymeric matrix and to investigate their behavior at different temperatures, thereby providing deeper insight into their molecular-level structural dynamics. To achieve this, the free terpyridine monomer (**Tpy-MA**), as well as the zinc and iron model complexes, $[(\text{Tpy})_2\text{Zn}]^{2+}$ and $[(\text{Tpy})_2\text{Fe}]^{2+}$ were first investigated to identify characteristic vibrational bands

that could serve as marker bands to confirm whether $\text{Zn}(\text{TFMS})_2$ or FeSO_4 metal salts successfully complex with the terpyridine ligand. Upon complexation, significant Raman spectral changes were observed, particularly in the zinc complex $[(\text{Tpy})_2\text{Zn}]^{2+}$, where the most pronounced changes occurred (Fig. S126). For instance, the Raman band at 339 cm^{-1} in free **Tpy-MA** spectrum is shifted to 349 cm^{-1} in the zinc complex, $[(\text{Tpy})_2\text{Zn}]^{2+}$, accompanied by the appearance of a new band at 313 cm^{-1}, forming a doublet attributed to the N–Zn stretching vibration.[146] A higher intensity and slight shifting of the above-mentioned band can also be seen in the DFT modeled Raman spectra (see SI, Fig. S147 and S148) supporting the experimental results. Here the band at approximately 324 cm^{-1} for the free ligand is shifted to 326 cm^{-1} with a much higher intensity for the bis-terpyridine zinc complex. In contrast, iron complexation results in a broad band at 310 cm^{-1} (see Fig. S126) corresponding to N–Fe stretching vibrations. These shifts occur due to coordination of the terpyridine nitrogen to the metal center, where the metal accepts additional electrons density from the terpyridine ligand. This electron transfer also quenches the intense δ(C–C) band at 997 cm^{-1} observed in the free **Tpy-MA** spectrum, resulting in a significant reduction in intensity for $[(\text{Tpy})_2\text{Fe}]^{2+}$ and almost complete disappearance in $[(\text{Tpy})_2\text{Zn}]^{2+}$. This phenomenon can also be seen in Fig. S147 and S148 of the modeled spectra where the mentioned band for the free terpyridine ligand disappears for both complexes. The weak doublet at 457 cm^{-1} and 469 cm^{-1} in the free **Tpy-MA** spectrum merges into a broader band at about 461 cm^{-1} in $[(\text{Tpy})_2\text{Fe}]^{2+}$, reflecting the distinct electronic and geometric environment introduced by iron complexation. This band is assigned to the N–Fe stretching vibration.[146,147] Moving to the higher wavenumbers, the Raman band at 644 cm^{-1} intensifies and blueshifts by approximately 6 cm^{-1} for both zinc and iron complexes. Meanwhile, the band at 623 cm^{-1} shifts to 639 cm^{-1} in the zinc complex and appears as a shoulder in the iron complex. In the breathing modes spectral range, the δ(C–C)

and δ(C–H) bands at 1030 cm^{-1} and 1041 cm^{-1} shifts and intensify to 1020 cm^{-1} and 1030 cm^{-1} for the zinc complex and 1023 cm^{-1} and 1039 cm^{-1} for the iron complex. The higher wavenumber shift and the intensification of the 1023 cm^{-1} band in the iron complex, suggests a stronger coordination of the terpyridine ligand to Fe^{2+} than to Zn^{2+}, which is in line with the ITC results mentioned above.[147] The described shifts are also visible in the modeled spectra, where at approximately 1020 cm^{-1} a significant increase in intensity for both complexes is visible. At even higher wavenumbers, the ν_{as}(C–C) band at 1201 cm^{-1} shifts and merges with another ν_{as}(C–C) band at 1251 cm^{-1} to form a single band at 1264 cm^{-1} in the zinc complex. This merging is likely due to mode coupling during zinc coordination. In contrast, a new band emerges at 1289 cm^{-1} in the iron complex, indicating a unique vibrational mode that arises exclusively from the iron coordination corresponding to a newly formed band for the C–C bond.[148] The ν(N–C) broad band at about 1400 cm^{-1} also undergoes significant changes, broadening into two bands centered at 1435 cm^{-1}. The symmetric doublet ν(CNC, C–C) at 1446 cm^{-1} and 1568 cm^{-1} shifts to 1474 cm^{-1} and 1499 cm^{-1} in the zinc complex and to 1469 cm^{-1} in the iron complex.

Additionally, the ν(CC, CN) band at 1356 cm^{-1} shifts by +12 cm^{-1} in the zinc complex and by +6 cm^{-1} in the iron complex. These shifts arise due to geometrical changes and mode coupling effects during complexation.[146] Furthermore, complex changes in the ν(CN, CC) region between 1550 and 1650 cm^{-1} were observed, which might be attributed to *cis*-to-*trans* transformations during complex formation.[145,146,149] A comparison of the determined band positions of the metal complexes by Raman and by DFT calculations can be found in the SI Table S14. To ensure that these identified characteristic bands can be used for validation, the ligand-containing polymers (**P1**, **P2**, and **P3**) without the metal complexes were analyzed to check for similarities. The analysis revealed that most of the identified bands can reliably confirm the presence of the complexes. However, the bands at 639 cm^{-1}, 700 cm^{-1}, 1030 cm^{-1} (zinc complex) and 1039 cm^{-1} (iron complex), and the region 1550 cm^{-1} to 1650 cm^{-1} overlaps with the polymer matrix, making them unsuitable for validation. The metallopolymers were subsequently measured and analyzed to validate the formation of the metal complexes. As shown in Fig. 5A and B for the iron and zinc-based metallopolymers, respectively, the identified characteristic Raman bands indicative for com-
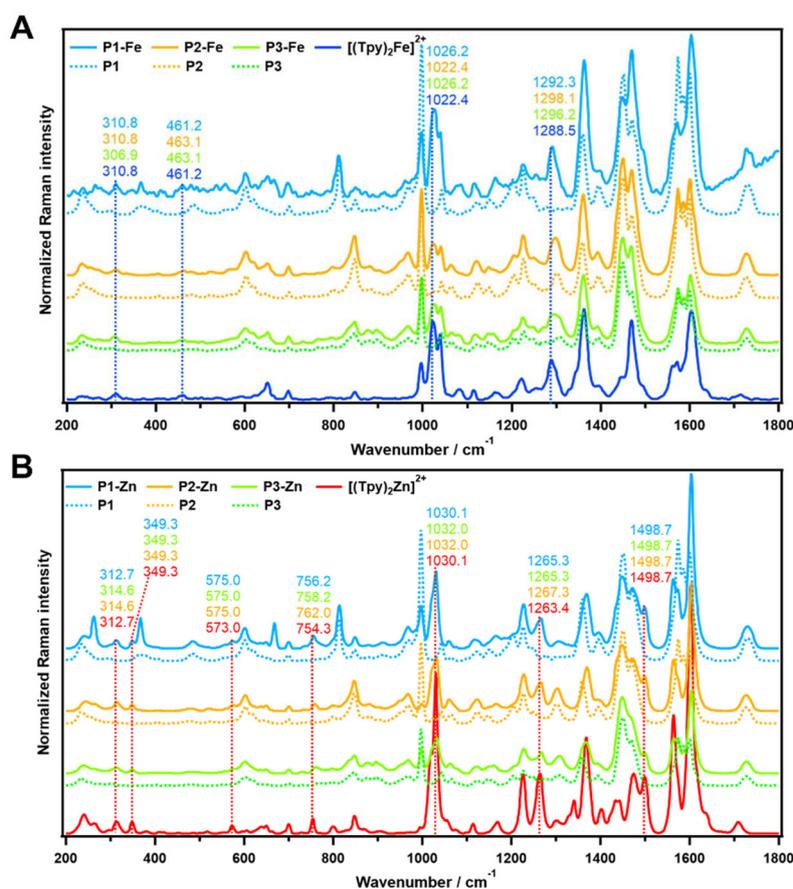

Fig. 5 Normalized FT-Raman spectra of the linear polymers **P1**, **P2** and **P3** and (A) Fe-complexed and (B) Zn-complexed metallopolymers showing the band positions of the identified characteristic peaks for validation.

plexation, as described above, were consistently present across all metallopolymers. Some bands exhibited shifts of up to +5 cm^{-1}, while others remain unchanged (localized and unaffected by the polymeric matrix). Additionally, broadening of certain vibrational modes, such as the band at 1264 cm^{-1}, the band at 754 cm^{-1}, and even the N–Zn band at 313 cm^{-1}, was observed. This broadening and shifting are attributed to the influence of the polymeric environment on the vibrational modes. Furthermore, it was observed with the **P1-Zn** metallopolymer that new bands emerged outside the previously identified characteristic bands following complexation. These new bands appear at approximately 263 cm^{-1}, 367 cm^{-1}, and 667 cm^{-1} and were also observed in the crosslinked polymer **P1-cc**, although their signal intensities were weak, with the exception of the 367 cm^{-1} band (see SI Fig. S140). The bands at 263 cm^{-1} and 367 cm^{-1} corresponds to C–C/C–O out of plane bending, while the band at 667 cm^{-1} is attributed to the wagging vibration of the C=O in the ester moiety of the methacrylate.[150–152] Upon complexation, these signals become significantly more intense, displaying almost equal intensities showing an influence of the metal complex spectrum by the presence of the surrounding polymer. Afterwards, temperature-dependent Raman measurements were conducted with a focus of the complexed metallopolymers **P1-Fe** to **P3-Zn**. Interestingly, during these measurements, the intensities of the complexation sensitive Raman bands decreased as the temperature increased (see SI, Fig. S141). This can be attributed to the fact that an increase in temperature disrupts the influence of the polymer environment on the coordination of the metal complex. However, the band positions remained relatively unchanged, except for the 667 cm^{-1} band, which shifted slightly to 665 cm^{-1} at 130 °C and further to 663 cm^{-1} at 140 °C and 150 °C. This might suggest a subtle change in the coordination environment and its geometry and also corresponds to the changes observed in the rheology at those temperatures. Thus, these changes in the molecular pattern fits to the observed reversibility in the frequency sweeps (and in the TTS) for the zinc complexes. The characteristic ν(Zn–N) bands at 312 cm^{-1} and 349 cm^{-1} showed minimal shifts in peak position for increasing temperature, highlighting the stability of the metal–ligand complex even at elevated temperatures. This finding corresponds perfectly to the DMTA measurements, in which G' is also higher than G''. Specifically, at 140 °C, the band at 312 cm^{-1} slightly shifts to 310 cm^{-1} before returning to 312 cm^{-1} at 150 °C. The 349 cm^{-1} band also exhibited minor back-and-forth shifts of 2 cm^{-1} starting from 70 °C. It should be noted that these fluctuations do not follow any observable trend, suggesting that the complex remains stable and localized, with no significant structural change in the metal complex. Similar characteristics were observed for the Zn–N vibration bands in the other metallopolymers, **P2-Zn** and **P3-Zn** (see SI, Fig. S142, S143 and Table S12 for the Raman band positions with respect to temperature.) The temperature-dependent Raman analysis shows that the observed Raman spectral changes arise primarily from thermally induced morphological changes in the polymer matrix

and localized vibrational changes in the coordination environment of the Zn^{2+} ions, while the terpyridine-zinc complex itself remains intact. This suggests a molecular mechanism that enables the reversible behavior of the metallopolymers. The finding is well in line with the DMTA measurements, which suggest a polymer network even at higher temperatures and no opening of the bonds (which would correspond to a dissociative mechanism). However, the dynamic behavior in the frequency-dependent measurements might be explainable with these structural changes observed in the temperature-dependent Raman measurements, since the reversibility by exchange reaction will presumably lead to a change in the molecular environment of the metal complexes. Alternatively, it could also be possible that certain aggregates, *e.g.*, ionic clusters are formed and the thermal treatment would lead to an exchange/reversibility of these. Such aggregates are known for supramolecular polymers containing polar groups in a non-polar polymer environment.[55,86,97,153,154] Fig. S144 through S146 illustrates the temperature-dependent Raman spectra of the **P1-Fe**, **P2-Fe**, and **P3-Fe** metallopolymers, respectively. Unfortunately, a significant loss in spectra intensity is observed for **P1-Fe** and **P2-Fe** at temperatures above 80 °C, while **P3-Fe** exhibits a similar decline beginning at around 100 °C. Here, the decline in intensity could be correlated to a temperature-dependent process that leads to environmental changes in the polymer network without significantly influencing the chemical structure. Sample degradation could be excluded, which was proven by the TGA and rheology measurements indicating stability of the metallopolymers at these high temperatures. Thus, these polymers could not be investigated in detail by temperature-dependent Raman measurements.

Conclusions

In the current study, our aim was to understand and describe the structural changes happening in metallopolymers. We therefore prepared metallopolymers containing terpyridine moieties as ligands in the side chains that form homoleptic complexes with Fe(ɪɪ) or Zn(ɪɪ) ions. The metallopolymers were characterized using DSC, TGA and elemental analysis. Rheological investigations were conducted, focusing on DMTA, stress relaxation, frequency sweeps and the TTS principle. Herein we concluded that frequency sweeps are the best method to characterize structural changes in such metallopolymers. Here it was possible to observe crossovers in the plots for the zinc containing bis-terpyridine complexes, which is well aligned with the higher reversibility of this bond. Stress relaxation measurements revealed activation energies of the overall relaxation process (*i.e.* polymer matrix and metal complexes). Furthermore, computational rheology was applied to construct master curves and relaxation spectra. Here it was possible to see different relaxation modes for the Fe(ɪɪ) and Zn(ɪɪ) containing metallopolymers clearly indicating a reversibility/relaxation caused by the metal complexes. For further investigation, Raman spectroscopy and DFT calculations were con-

ducted. The formation of the complexes could be demonstrated with both methods, and temperature-dependent Raman spectroscopy revealed no significant structural changes of the metal complexes but rather a thermal-induced morphological change of the polymer matrix. These findings align with the DMTA measurements, where no dissociation of the bonds of the polymer network could be observed. The frequency-dependent dynamics may stem from reversible structural changes, which are also observable in the temperature-dependent Raman spectra, likely due to exchange reactions of metal complexes or exchanges within certain aggregates.

Overall, this study demonstrates that dynamic metallopolymers can be comprehensively characterized using a combination of complementary analytical techniques. In particular, DMTA, frequency-dependent measurements and TTS are very useful rheological approaches, whereas Raman spectroscopy in combination with DFT calculations provides valuable insights into the molecular structure.

In future studies, other ligands and metal salts should be studied to investigate their structural behavior and see if those changes occur only within the polymer matrix or within metal complexes inside the metallopolymers.

Author contributions

Synthesis of monomer, polymers and metallopolymers: M. J.; SEC, DSC, TGA: M. J.; rheology measurements: M. J.; Raman measurements: M. F. A.; DFT calculations: W. T. S., C. W.; RheoSpec: J. K.; ITC-measurements: T. B.; writing of the manuscript: M. J., M. F. A., S. Z.; interpretation of data: M. J., M. F. A., S. Z., M. S.; supervision: S. Z., A. C., M. S., J. P., S. G., M. D. H., U. S. S.; concept of the study: S. Z., M. D. H., U. S. S.; correction of the manuscript: S. Z., A. C., M. S., J. P., S. G., M. D. H., U. S. S.; funding: J. P., S. G., M. D. H., U. S. S.

Conflicts of interest

There are no conflicts to declare.

Data availability

The data supporting this article is included in the supplementary information (SI). Supplementary information: information about the used chemicals and instruments, the synthesis of the polymers, metallopolymers and polymer networks as well as detailed information about the characterization of those, *e.g.*, NMR, SEC, DSC, TGA and elemental analysis data and curves. Additionally, the plots of the DMTA, frequency sweeps, stress relaxation, Arrhenius and TTS; the measured Raman spectra as well as the DFT modeled Raman spectra. See DOI: https://doi.org/10.1039/d6py00053c.

All primary data can be found under the following https://doi.org/10.5281/zenodo.18182255.

Acknowledgements

References

1 D. Hao, G. R. Asrar, Y. Zeng, X. Yang, X. Li, J. Xiao, K. Guan, J. Wen, Q. Xiao, J. A. Berry and M. Chen, *Global Change Biol.*, 2021, **27**, 2144–2158.

2 C. Ciaccio, A. Coletta and M. Coletta, *Mol. Aspects Med.*, 2022, **84**, 101022.

3 R. M. Winslow, *Respir. Physiol. Neurobiol.*, 2007, **158**, 121–127.

4 M. B. Oliveira and J. F. Mano, *Biotechnol. Prog.*, 2011, **27**, 897–912.

5 A. Göthlich, S. Koltzenburg and G. Schornick, *Chem. Unserer Zeit*, 2005, **39**, 262–273.

6 K. Lee, J. Y. Kim, S. H. Park, S. H. Kim, S. Cho and A. J. Heeger, *Adv. Mater.*, 2007, **19**, 2445–2449.

7 N. Roy, B. Bruchmann and J.-M. Lehn, *Chem. Soc. Rev.*, 2015, **44**, 3786–3807.

8 F. Liu and M. W. Urban, *Prog. Polym. Sci.*, 2010, **35**, 3–23.

9 M. Wei, Y. Gao, X. Li and M. J. Serpe, *Polym. Chem.*, 2017, **8**, 127–143.

10 A. Bratek-Skicki, *Appl. Surf. Sci. Adv.*, 2021, **4**, 100068.

11 F. García and M. M. J. Smulders, *J. Polym. Sci., Part A: Polym. Chem.*, 2016, **54**, 3551–3577.

12 Y. Yang and M. W. Urban, *Adv. Mater. Interfaces*, 2018, **5**, 1800384.

13 S. J. Rowan, S. J. Cantrill, G. R. L. Cousins, J. K. M. Sanders and J. F. Stoddart, *Angew. Chem., Int. Ed.*, 2002, **41**, 898–952.

14 Y. Chujo, K. Sada and T. Saegusa, *Macromolecules*, 1990, **23**, 2636–2641.

15 S. Terryn, J. Brancart, E. Roels, R. Verhelle, A. Safaei, A. Cuvellier, B. Vanderborght and G. Van Assche, *Macromolecules*, 2022, **55**, 5497–5513.

16 W. T. Schulze, S. Schwalbe, K. Trepte, A. Croy, J. Kortus and S. Gräfe, *J. Chem. Phys.*, 2023, **158**, 164102.

17 B. Zhou, T. Deng, C. Yang, M. Wang, H. Yan, Z. Yang, Z. Wang and Z. Xue, *Adv. Funct. Mater.*, 2023, **33**, 2212005.

18 O. R. Cromwell, J. Chung and Z. Guan, *J. Am. Chem. Soc.*, 2015, **137**, 6492–6495.

19 C. Kim, H. Ejima and N. Yoshie, *J. Mater. Chem. A*, 2018, **6**, 19643–19652.

20 J. J. Cash, T. Kubo, A. P. Bapat and B. S. Sumerlin, *Macromolecules*, 2015, **48**, 2098–2106.

21 H. Otsuka, K. Aotani, Y. Higaki, Y. Amamoto and A. Takahara, *Macromolecules*, 2007, **40**, 1429–1434.

22 M. Aiba, T. Higashihara, M. Ashizawa, H. Otsuka and H. Matsumoto, *Macromolecules*, 2016, **49**, 2153–2161.

23 A. Chao, I. Negulescu and D. Zhang, *Macromolecules*, 2016, **49**, 6277–6284.

24 G. P. Carden, M. L. Martins, G. Toleutay, S. Ge, B. Li, S. Zhao and A. P. Sokolov, *Macromolecules*, 2024, **57**, 8621–8631.

25 H. Otsuka, S. Nagano, Y. Kobashi, T. Maeda and A. Takahara, *Chem. Commun.*, 2010, **46**, 1150–1152.

26 Q. Zhang, D.-H. Qu, B. L. Feringa and H. Tian, *J. Am. Chem. Soc.*, 2022, **144**, 2022–2033.

27 Y. Li, Y. Wang, S. Wang, Z. Ye, C. Bian, X. Xing, T. Hong and X. Jing, *Macromolecules*, 2022, **55**, 9091–9102.

28 M. A. Bin Rusayyis and J. M. Torkelson, *ACS Macro Lett.*, 2022, **11**, 568–574.

29 C. Du, X. N. Zhang, T. L. Sun, M. Du, Q. Zheng and Z. L. Wu, *Macromolecules*, 2021, **54**, 4313–4325.

30 Z. Zhou, S. Chen, X. Xu, Y. Chen, L. Xu, Y. Zeng and F. Zhang, *Prog. Org. Coat.*, 2021, **154**, 106213.

31 R. Bai, H. Zhang, X. Yang, J. Zhao, Y. Wang, Z. Zhang and X. Yan, *Polym. Chem.*, 2022, **13**, 1253–1259.

32 Y. Liu, J. Wan, X. Zhao, J. Zhao, Y. Guo, R. Bai, Z. Zhang, W. Yu, H. W. Gibson and X. Yan, *Angew. Chem., Int. Ed.*, 2023, **62**, e202302370.

33 J. Dai, Z. Wang, Z. Wu, Z. Fang, S. Heliu, W. Yang, Y. Bai and X. Zhang, *ACS Appl. Polym. Mater.*, 2023, **5**, 2575–2582.

34 X. Yuan, X. Lin, F. Dong, X. Huang, H. Liu and X. Xu, *ACS Appl. Polym. Mater.*, 2025, **7**, 1328–1337.

35 D. Zhao, J. Yang, X. Tian, J. Wei, Q. Li and Y. Wang, *Chem. Eng. J.*, 2022, **434**, 134806.

36 G. Chen, B. Jin, Q. Zhao and T. Xie, *J. Mater. Chem. A*, 2021, **9**, 6827–6830.

37 A. W. Bosman, R. P. Sijbesma and E. W. Meijer, *Mater. Today*, 2004, **7**, 34–39.

38 P. Ximenis, D. Martínez, L. Rubert and B. Soberats, *Chem. Soc. Rev.*, 2025, **54**, 11659–11698.

39 H.-J. Schneider and A. K. Yatsimirsky, *Chem. Soc. Rev.*, 2008, **37**, 263–277.

40 Y. Zhu, W. Zheng, W. Wang and H.-B. Yang, *Chem. Soc. Rev.*, 2021, **50**, 7395–7417.

41 D. Mozhdehi, J. A. Neal, S. C. Grindy, Y. Cordeau, S. Ayala, N. Holten-Andersen and Z. Guan, *Macromolecules*, 2016, **49**, 6310–6321.

42 J. Meurer, J. Hniopek, T. Bätz, S. Zechel, M. Enke, J. Vitz, M. Schmitt, J. Popp, M. D. Hager and U. S. Schubert, *Adv. Mater.*, 2021, **33**, 2006655.

43 A. C. Jackson, F. L. Beyer, S. C. Price, B. C. Rinderspacher and R. H. Lambeth, *Macromolecules*, 2013, **46**, 5416–5422.

44 R. D. Mukhopadhyay and A. Ajayaghosh, *Chem. Soc. Rev.*, 2023, **52**, 8635–8650.

45 S. Götz, S. Zechel, M. D. Hager, G. R. Newkome and U. S. Schubert, *Prog. Polym. Sci.*, 2021, **119**, 101428.

46 Y. Yao, S. Jin, H. Zou, L. Li, X. Ma, G. Lv, F. Gao, X. Lv and Q. Shu, *J. Mater. Sci.*, 2021, **56**, 6549–6580.

47 K. P. Nair, V. Breedveld and M. Weck, *Macromolecules*, 2008, **41**, 3429–3438.

48 C. Sun, F. Pan, H. Bin, J. Zhang, L. Xue, B. Qiu, Z. Wei, Z.-G. Zhang and Y. Li, *Nat. Commun.*, 2018, **9**, 743.

49 K. C. Gupta and A. K. Sutar, *Coord. Chem. Rev.*, 2008, **252**, 1420–1450.

50 D.-L. Ma, H.-Z. He, K.-H. Leung, D. S.-H. Chan and C.-H. Leung, *Angew. Chem., Int. Ed.*, 2013, **52**, 7666–7682.

51 A. R. Yaul, V. V. Dhande, G. B. Pethe and A. S. Aswar, *Bull. Chem. Soc. Ethiop.*, 2014, **28**, 255–264.

52 Y. Liu, S.-C. Yiu, C.-L. Ho and W.-Y. Wong, *Coord. Chem. Rev.*, 2018, **375**, 514–557.

53 Y. Sekine, R. Akiyoshi and S. Hayami, *Coord. Chem. Rev.*, 2022, **469**, 214663.

54 S. D. Bella, *Chem. Soc. Rev.*, 2001, **30**, 355–366.

55 B. Sandmann, S. Bode, M. D. Hager and U. S. Schubert, in *Adv. Polym. Sci*, ed. V. Percec, Springer International Publishing, Cham, 2013, pp. 239–257.

56 S. Bode, R. K. Bose, S. Matthes, M. Ehrhardt, A. Seifert, F. H. Schacher, R. M. Paulus, S. Stumpf, B. Sandmann, J. Vitz, A. Winter, S. Hoeppener, S. J. Garcia, S. Spange, S. van der Zwaag, M. D. Hager and U. S. Schubert, *Polym. Chem.*, 2013, **4**, 4966–4973.

57 J. Meurer, T. Bätz, J. Hniopek, S. Zechel, M. Schmitt, J. Popp, M. D. Hager and U. S. Schubert, *J. Mater. Chem. A*, 2021, **9**, 15051–15058.

58 J. Meurer, T. Bätz, J. Hniopek, M. Jäger, S. Zechel, M. Schmitt, J. Popp, M. D. Hager and U. S. Schubert, *Polymers*, 2022, **14**, 1833.

59 F. Ciardelli, E. Tsuchida and D. Wöhrle, in *Macromolecule-Metal Complexes*, Springer, Berlin, Heidelberg, 1996.

60 A. Wild, A. Winter, F. Schlütter and U. S. Schubert, *Chem. Soc. Rev.*, 2011, **40**, 1459–1511.

61 W.-Y. Wong, S.-M. Chan, K.-H. Choi, K.-W. Cheah and W.-K. Chan, *Macromol. Rapid Commun.*, 2000, **21**, 453–457.

62 P. Yang, P. Pageni, M. P. Kabir, T. Zhu and C. Tang, *ACS Macro Lett.*, 2016, **5**, 1293–1300.

63 S. Bode, M. Enke, R. K. Bose, F. H. Schacher, S. J. Garcia, S. van der Zwaag, M. D. Hager and U. S. Schubert, *J. Mater. Chem. A*, 2015, **3**, 22145–22153.

64 S. Götz, M. Abend, S. Zechel, M. D. Hager and U. S. Schubert, *J. Appl. Polym. Sci.*, 2019, **136**, 47064.

65 T. Bätz, H. H. Haeri, S. Langstein, S. Zechel, M. D. Hager, D. Hinderberger and U. S. Schubert, *Polymer*, 2024, **307**, 127258.

66 M. Enke, S. Bode, J. Vitz, F. H. Schacher, M. J. Harrington, M. D. Hager and U. S. Schubert, *Polymer*, 2015, **69**, 274–282.

67 W. Bian, H. Lian, Y. Zhang, F. Tai, H. Wang, Q. Dong, B. Yu, X. Wei and Q. Zhao, *J. Organomet. Chem.*, 2017, **835**, 25–30.

68 C. F. Pereira, A. Olean-Oliveira, D. N. David-Parra and M. F. S. Teixeira, *Talanta*, 2018, **190**, 119–125.

69 J. Polozhentseva, M. Novozhilova and M. Karushev, *Int. J. Mol. Sci.*, 2022, **23**, 1795.

70 H. Zhan, S. Lamare, A. Ng, T. Kenny, H. Guernon, W.-K. Chan, A. B. Djurišić, P. D. Harvey and W.-Y. Wong, *Macromolecules*, 2011, **44**, 5155–5167.

71 M. Ahmadi, C. Sprenger, G. Pareras, A. Poater and S. Seiffert, *Soft Matter*, 2023, **19**, 8112–8123.

72 R. Dobrawa and F. Würthner, *J. Polym. Sci., Part A:Polym. Chem.*, 2005, **43**, 4981–4995.

73 K. N. Aziz, K. M. Ahmed, R. A. Omer, A. F. Qader and E. I. Abdulkareem, *Rev. Inorg. Chem.*, 2025, **45**, 1–19.

74 A. Kumar, S. Bawa, J. Bera, U. Shankar, S. Sahu and A. Bandyopadhyay, *J. Appl. Polym. Sci.*, 2023, **140**, e53242.

75 J. Fritsch, D. Mansfeld, M. Mehring, R. Wursche, J. Grothe and S. Kaskel, *Polymer*, 2011, **52**, 3263–3268.

76 Y. Liang, D. Strohecker, V. Lynch, B. J. Holliday and R. A. Jones, *ACS Appl. Mater. Interfaces*, 2016, **8**, 34568–34580.

77 J. J. Walsh, Q. Zeng, R. J. Forster and T. E. Keyes, *Photochem. Photobiol. Sci.*, 2012, **11**, 1547–1557.

78 Z. Zhang, Y.-N. He, L. Liu, X.-Q. Lü, X.-J. Zhu, W.-K. Wong, M. Pan and C.-Y. Su, *Chem. Commun.*, 2016, **52**, 3713–3716.

79 W.-X. Feng, S.-Y. Yin, M. Pan, H.-P. Wang, Y.-N. Fan, X.-Q. Lü and C.-Y. Su, *J. Mater. Chem. C*, 2017, **5**, 1742–1750.

80 D. Zhao, L. Guo, Q. Li, C. Yue, B. Han, K. Liu and H. Li, *Adv. Mater.*, 2024, **36**, 2405164.

81 N. Hannewald, M. Enke, I. Nischang, S. Zechel, M. D. Hager and U. S. Schubert, *J. Inorg. Organomet. Polym. Mater.*, 2020, **30**, 230–242.

82 H. A. Barnes, *Rheol. Rev.*, 2003, 1–36.

83 T. Okada, K. Komatsu, T. Kawamoto, T. Yamanaka and H. Kagi, *Spectrochim. Acta, Part A*, 2005, **61**, 2423–2427.

84 O. C. Adekoya, G. J. Adekoya, E. R. Sadiku, Y. Hamam and S. S. Ray, *Pharmaceutics*, 2022, **14**, 1972.

85 J. Meurer, T. Bätz, J. Hniopek, C. Bernt, S. Zechel, M. Schmitt, J. Popp, M. D. Hager and U. S. Schubert, *J. Mater. Chem. A*, 2022, **10**, 25106–25117.

86 S. Bode, L. Zedler, F. H. Schacher, B. Dietzek, M. Schmitt, J. Popp, M. D. Hager and U. S. Schubert, *Adv. Mater.*, 2013, **25**, 1634–1638.

87 C. Wei, Y. He, X. Shi and Z. Song, *Coord. Chem. Rev.*, 2019, **385**, 1–19.

88 U. S. Schubert and C. Eschbaumer, *Angew. Chem., Int. Ed.*, 2002, **41**, 2892–2926.

89 L. Leibler, M. Rubinstein and R. H. Colby, *Macromolecules*, 1991, **24**, 4701–4707.

90 H. Chen, R. Shi and H. Ow, *ACS Omega*, 2019, **4**, 20665–20671.

91 O. Gutten, I. Beššeová and L. Rulíšek, *J. Phys. Chem. A*, 2011, **115**, 11394–11402.

92 O. Gutten and L. Rulíšek, *Inorg. Chem.*, 2013, **52**, 10347–10355.

93 D. M. Parragh, C. Scheuerlein, N. Martin, R. Piccin, F. Ravotti, G. Pezzullo, T. Koettig and D. Lellinger, *Polymers*, 2024, **16**, 407.

94 T. Mezger, in *Angewandte Rheologie: Mit Joe Flow auf der Rheologie-Straße*, Anton Paar GmbH, Graz, 2017, pp. 9833–9841.

95 H. Zhang, D. Wang, N. Wu, C. Li, C. Zhu, N. Zhao and J. Xu, *ACS Appl. Mater. Interfaces*, 2020, **12**, 9833–9841.

96 R. K. Bose, N. Hohlbein, S. J. Garcia, A. M. Schmidt and S. van der Zwaag, *Phys. Chem. Chem. Phys.*, 2014, **17**, 1697–1704.

97 S. Chen and W. H. Binder, *Acc. Chem. Res.*, 2016, **49**, 1409–1420.

98 S. Ge, Y.-H. Tsao and C. M. Evans, *Nat. Commun.*, 2023, **14**, 7244.

99 J. Zhao, Z. Zhang, C. Wang and X. Yan, *CCS Chem.*, 2023, **6**, 41–56.

100 V. Zhang, B. Kang, J. V. Accardo and J. A. Kalow, *J. Am. Chem. Soc.*, 2022, **144**, 22358–22377.

101 C. Taplan, M. Guerre and F. E. Du Prez, *J. Am. Chem. Soc.*, 2021, **143**, 9140–9150.

102 X. Kuang, G. Liu, X. Dong and D. Wang, *Mater. Chem. Front.*, 2016, **1**, 111–118.

103 S. Xu, D. Sheng, Y. Zhou, H. Wu, H. Xie, X. Tian, Y. Sun, X. Liu and Y. Yang, *New J. Chem.*, 2020, **44**, 7395–7400.

104 Y. Vidavsky, M. R. Buche, Z. M. Sparrow, X. Zhang, S. J. Yang, R. A. DiStasio Jr. and M. N. Silberstein, *Macromolecules*, 2020, **53**, 2021–2030.

105 R. D. Sudduth, *J. Appl. Polym. Sci.*, 2001, **82**, 527–540.

106 D. Berne, S. Laviéville, E. Leclerc, S. Caillol, V. Ladmiral and C. Bakkali-Hassani, *ACS Polym. Au*, 2025, **5**, 214–240.

107 Q. Peng, Z. Zhu, C. Jiang and H. Jiang, *Adv. Ind. Eng. Polym. Res.*, 2019, **2**, 61–68.

108 W. Denissen, J. M. Winne and F. E. D. Prez, *Chem. Sci.*, 2015, **7**, 30–38.

109 F. Meng, M. O. Saed and E. M. Terentjev, *Macromolecules*, 2019, **52**, 7423–7429.

110 L. E. Porath and C. M. Evans, *Macromolecules*, 2021, **54**, 4782–4791.

111 N. Rabiei, S. H. Amirshahi and M. Haghighat Kish, *Phys. Rev. E*, 2019, **99**, 032502.

112 N. Nishiie, R. Kawatani, S. Tezuka, M. Mizuma, M. Hayashi and Y. Kohsaka, *Nat. Commun.*, 2024, **15**, 8657.

113 M. Capelot, M. M. Unterlass, F. Tournilhac and L. Leibler, *ACS Macro Lett.*, 2012, **1**, 789–792.

114 M. Guerre, C. Taplan, J. M. Winne and F. E. Du Prez, *Chem. Sci.*, 2020, **11**, 4855–4870.

115 M. L. Martins, X. Zhao, Z. Demchuk, J. Luo, G. P. Carden, G. Toleutay and A. P. Sokolov, *Macromolecules*, 2023, **56**, 8688–8696.

116 J. Dealy and D. Plazek, *Rheol. Bull.*, 2009, **78**, 16–31.

117 R. G. Ricarte and S. Shanbhag, *Polym. Chem.*, 2024, **15**, 815–846.

118 L.-I. Palade, V. Verney and P. Attané, *Rheol. Acta*, 1996, **35**, 265–273.

119 L. I. Palade, V. Verney and P. Attane, *Macromolecules*, 1995, **28**, 7051–7057.

120 F. Zhuge, J. Brassinne, C.-A. Fustin, E. van Ruymbeke and J.-F. Gohy, *Macromolecules*, 2017, **50**, 5165–5175.

121 R. J. Hickey, T. M. Gillard, M. T. Irwin, T. P. Lodge and F. S. Bates, *Soft Matter*, 2016, **12**, 53–66.

122 R. J. Sheridan and C. N. Bowman, *Macromolecules*, 2012, **45**, 7634–7641.

123 R. K. Bose, M. Enke, A. M. Grande, S. Zechel, F. H. Schacher, M. D. Hager, S. J. Garcia, U. S. Schubert and S. van der Zwaag, *Eur. Polym. J.*, 2017, **93**, 417–427.

124 R. Kampes, J. Meurer, J. Hniopek, C. Bernt, S. Zechel, M. Schmitt, J. Popp, M. D. Hager and U. S. Schubert, *Front. Soft Matter*, 2022, **2**, 14.

125 J.-E. Potaufeux, R. Tavernier, J. Odent and J.-M. Raquez, *Macromolecules*, 2024, **57**, 7884–7892.

126 H. Fang, X. Gao, F. Zhang, W. Zhou, G. Qi, K. Song, S. Cheng, Y. Ding and H. H. Winter, *Macromolecules*, 2022, **55**, 10900–10911.

127 C. D. Han and M. S. Jhon, *J. Appl. Polym. Sci.*, 1986, **32**, 3809–3840.

128 D. G. Fesko and N. W. Tschoegl, *J. Polym. Sci., Part C*, 1971, **35**, 51–69.

129 J. Ahmed, R. Auras, T. Kijchavengkul and S. K. Varshney, *J. Food Eng.*, 2012, **111**, 580–589.

130 C. Smithson, M. Stamenović, M. Nujkić and S. Putić, *Zast. Mater.*, 2014, **55**, 395–400.

131 P. A. O'Connell and G. B. McKenna, *J. Chem. Phys.*, 1999, **110**, 11054–11060.

132 J. Rault, *J. Non-Cryst. Solids*, 2000, **271**, 177–217.

133 M. L. Williams, R. F. Landel and J. D. Ferry, *J. Am. Chem. Soc.*, 1955, **77**, 3701–3707.

134 V. Montano, S. J. Picken, S. Van Der Zwaag and S. J. Garcia, *Phys. Chem. Chem. Phys.*, 2019, **21**, 10171–10184.

135 J. Honerkamp and J. Weese, *Rheol. Acta*, 1993, **32**, 65–73.

136 A. Stankiewicz, *Materials*, 2024, **17**, 1527.

137 J. Song, N. Holten-Andersen and G. H. McKinley, *Soft Matter*, 2023, **19**, 7885–7906.

138 L. Xi, R. Luo, Q. Ma, C. Tu and Y. I. Shah, *Constr. Build. Mater.*, 2022, **354**, 129182.

139 I. Emri and N. W. Tschoegl, *Rheol. Acta*, 1993, **32**, 311–322.

140 M. Baumgaertel and H. H. Winter, *Rheol. Acta*, 1989, **28**, 511–519.

141 C. S. Y. Tan, G. Agmon, J. Liu, D. Hoogland, E.-R. Janeček, E. A. Appel and O. A. Scherman, *Polym. Chem.*, 2017, **8**, 5336–5343.

142 P. Edera, S. Chappuis, M. Cloitre and F. Tournilhac, *Polymer*, 2024, **299**, 126916.

143 S. Ge, Y.-H. Tsao and C. M. Evans, *Nat. Commun.*, 2023, **14**, 7244.

144 V. Montano, M. Senardi, S. van der Zwaag and S. J. Garcia, *Phys. Chem. Chem. Phys.*, 2020, **22**, 21750–21760.

145 T. Bätz, M. F. Agyemang, J. Meurer, J. Hniopek, S. Zechel, M. Schmitt, J. Popp, M. D. Hager and U. S. Schubert, *Polym. Chem.*, 2025, **16**, 492–502.

146 M. Presselt, B. Dietzek, M. Schmitt, J. Popp, A. Winter, M. Chiper, C. Friebe and U. S. Schubert, *J. Phys. Chem. C*, 2008, **112**, 18651–18660.

147 I. Šloufová, B. Vlčková, P. Mojzeš, I. Matulková, I. Císařová, M. Procházka and J. Vohlídal, *J. Phys. Chem. C*, 2018, **122**, 6066–6077.

148 I. Šloufová, B. Vlčková, M. Procházka, J. Svoboda and J. Vohlídal, *J. Raman Spectrosc.*, 2014, **45**, 338–348.

149 J. Kožíšek, J. Svoboda, J. Zedník, B. Vlčková and I. Šloufová, *J. Phys. Chem. B*, 2021, **125**, 12847–12858.

150 G. Socrates, in *Infrared and Raman characteristic group frequencies: tables and charts*, Wiley, Chichester Weinheim, 3rd edn, 2001.

151 C. Apip, A. Martínez, M. Meléndrez, M. Domínguez, T. Marzialetti, R. Báez, G. Sánchez-Sanhueza, A. Jaramillo and A. Catalán, *Saudi Dent. J.*, 2021, **33**, 944–953.

152 M. Rosemal, H. Haris, K. Sathasivam and S. Mohan, *Pharm. Chem.*, 2010, **2**, 316–323.

153 A. Eisenberg, *Macromolecules*, 1970, **3**, 147–154.

154 F. Herbst, K. Schröter, I. Gunkel, S. Gröger, T. Thurn-Albrecht, J. Balbach and W. H. Binder, *Macromolecules*, 2010, **43**, 10006–10016.